

Supporting Information

(Fe, F) co-doped nickel oxyhydroxide for highly efficient oxygen evolution reaction

Jiajun Wang, Yanmei Ren and Ping Wang*

School of Materials Science and Engineering, South China University of Technology,

Guangzhou 510641, P. R. China

*Corresponding Author

E-mail: mspwang@scut.edu.cn (P. Wang)

Experimental Section

Fabrication of electrocatalyst

The commercial NF with an area density of $\sim 480 \text{ gm}^{-2}$ and a thickness of 1.6 mm was selected as conductive substrate to prepare a monolithic electrocatalyst. Prior to its usage, NF was cleaned following a standard procedure. The cleaned NF, together with 30 mL of 0.02 M $\text{NiSO}_4 \cdot 6\text{H}_2\text{O}$ solution, was transferred into a Teflon-lined stainless-steel autoclave and then heated at 160 °C for 5 h. The thus-prepared sample was cleaned and further annealed at 350 °C for 2 h under an Ar atmosphere. The anodic electrooxidation treatment was carried out at ambient temperature using a standard three-electrode cell with the NF-supported sample as the working electrode, graphite plates as counter electrode and Ag/AgCl (with 3.0 M KCl) as reference electrode. The electrooxidation operation was conducted in an aqueous solution of varied concentrations of KF and FeSO_4 at $5\sim 20 \text{ mA}\cdot\text{cm}^{-2}$ for a duration ranging from 0.5 to 1.5 h. The thus-prepared catalyst was carefully cleaned following the routine procedure. For comparison, the F-free or Fe-free electrocatalyst was synthesized under identical conditions except for the absence of KF or FeSO_4 in the electrolyte.

In preparation of the RuO_2/NF reference sample, 5 mg of powdery RuO_2 (99.9%) and 60 μL of 5 wt% Nafion solution were first ultrasonically dispersed in 1 mL of deionized water/ethanol mixture (4:1 v/v) for 1 h to form a homogeneous ink. 500 μL of the ink was then drop-cast onto the cleaned NF, and the resulting sample was finally dried at ambient temperature.

Characterization of catalyst

The catalyst samples were routinely characterized by X-ray diffraction (XRD, Rigaku MiniFlex 600), Field-emission scanning electron microscopy (FE-SEM, ZEISS MERLIN) and high-resolution transmission electron microscopy (HRTEM, JEOL-2100F). The surface chemical state analyses of the samples were conducted on a Thermo Scientific K-ALPHA⁺ X-ray photoelectron spectrometer (XPS) with all the binding energies calibrated by the C 1s peak (at 284.8 eV) of adventitious carbon. Raman spectra were recorded by a Thermo Scientific DXR microscope. The N₂ sorption isotherms of the samples were measured on a Micromeritics ASAP 2460 apparatus at 77 K. The synchrotron X-ray absorption fine structure (EXAFS) and X-ray absorption near edge structure (XANES) measurements were performed in BL17C beamline of the Synchrotron Radiation Research Center at Hsinchu, Taiwan. The XAFS raw data were processed using the ATHENA program. Least-squares fitting of the Fourier transformed EXAFS signals was carried out using IFEFFIT and the k^w -weighted $\chi(k)$ was Fourier-transformed to obtain R -space data.

Electrochemical measurements

In the present study, we conducted all electrochemical measurements on a CHI 660E workstation at room temperature using a three-electrode setup as described above. All electrochemical potentials were calibrated versus the reversible hydrogen electrode (RHE). The linear sweep voltammetry (LSV) polarization curves were measured in an O₂-saturated 1.0 M KOH solution over a potential range of 1.23~1.63 V versus RHE at a scan rate of 1 mV s⁻¹ with 95% iR compensation. EIS measurements were performed over a frequency range of 0.1 Hz to 100 kHz at open circuit potential

(OCP). The double-layer capacitances (C_{DL}) of the samples were determined by performing cyclic voltammetry (CV) in a non-Faradaic region at scan rates ranging from 10 to 60 mV s^{-1} . The Faradaic efficiency was evaluated based on the collected O_2 and H_2 volumes at the anode and cathode sides, respectively.

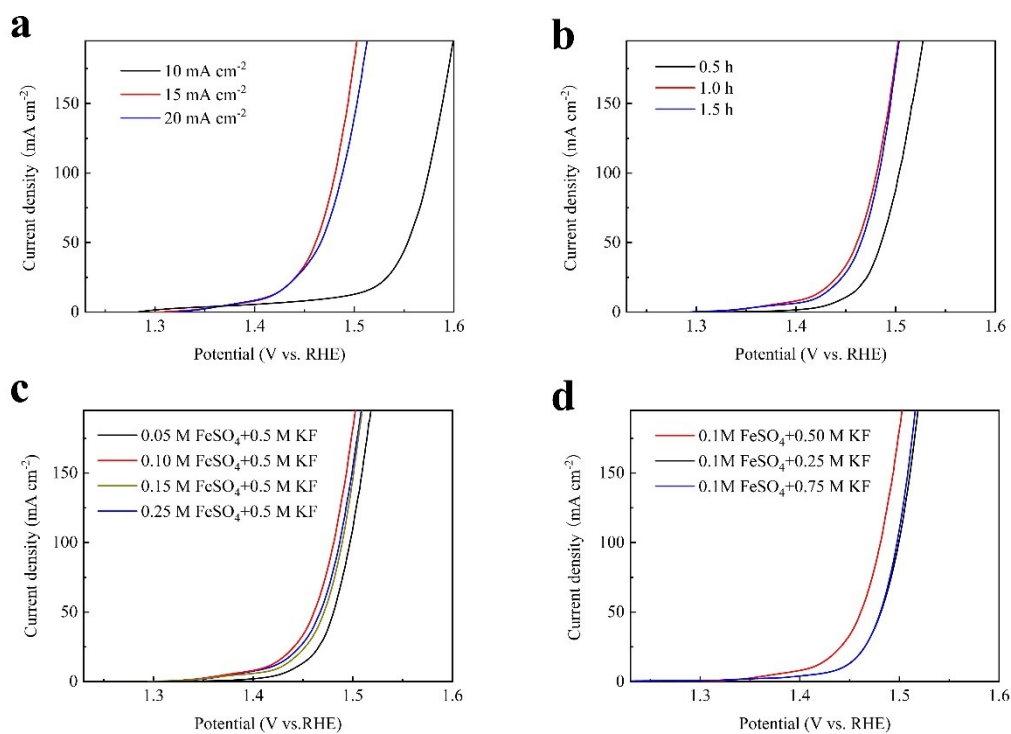


Fig. S1. OER polarization curves (with 95% iR compensation) of $\text{Ni}_{1-x}\text{Fe}_x\text{O}(\text{OH})_{1-y}\text{F}_y/\text{NiO}/\text{NF}$ catalysts that were prepared (a) at different current density; (b) at 15 mA cm^{-2} with different anodic electrooxidation duration; (c) at 15 mA cm^{-2} for 1 h in an electrolyte with different concentrations of FeSO_4 and a fixed concentration of KF (0.5M); (d) at 15 mA cm^{-2} for 1 h in an electrolyte with different concentrations of KF and a fixed concentration of FeSO_4 (0.1M).

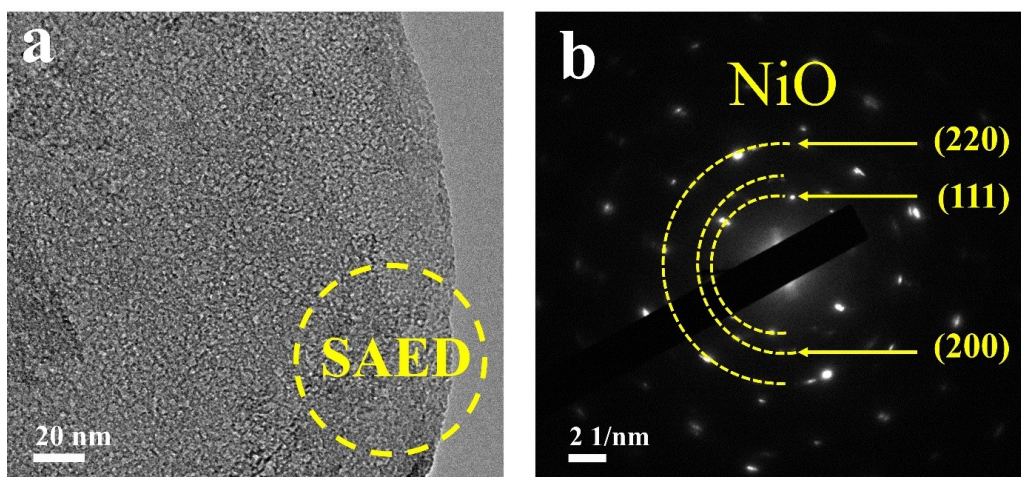


Fig. S2. (a) TEM image and (b) SAED pattern of the calcined sample..

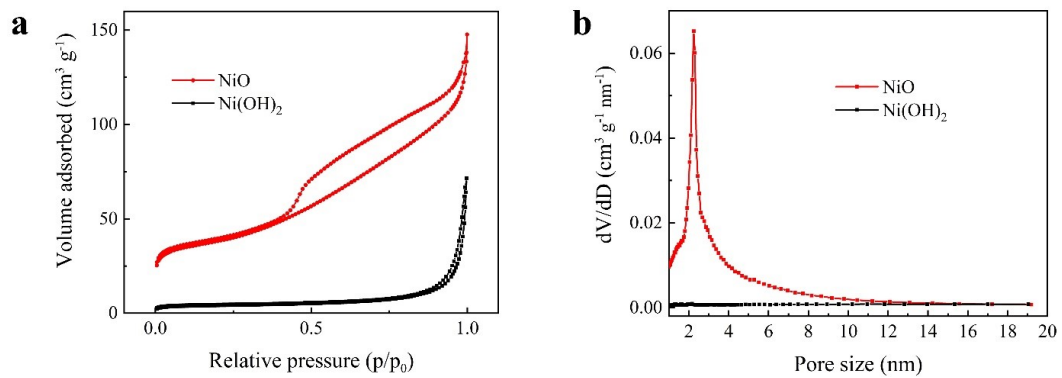


Fig. S3. (a) N₂ adsorption-desorption isotherms and (b) the corresponding pore size distribution of NiO and Ni(OH)₂ samples.

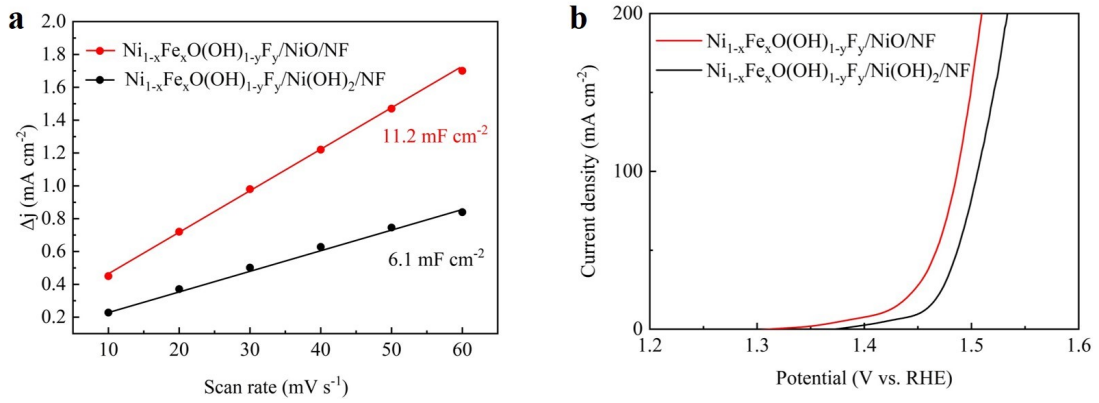


Fig. S4. (a) Capacitive current densities at OCP as a function of scan rate and (b) OER polarization curves (with 95% iR compensation) of Ni_{1-x}Fe_xO(OH)_{1-y}F_y/NiO/NF and Ni_{1-x}Fe_xO(OH)_{1-y}F_y/Ni(OH)₂/NF samples.

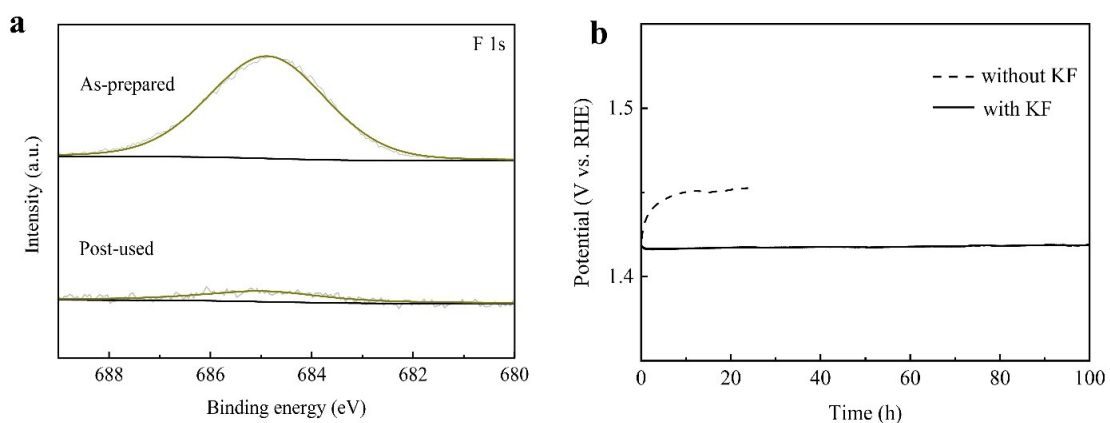


Fig. S5. (a) A comparison of the XPS F 1s spectra of $\text{Ni}_{1-x}\text{Fe}_x\text{O}(\text{OH})_{1-y}\text{F}_y/\text{NiO}/\text{NF}$ before and after long-term operation in a 1.0 M KOH solution, (b) Chronopotentiometric curves of $\text{Ni}_{1-x}\text{Fe}_x\text{O}(\text{OH})_{1-y}\text{F}_y/\text{NiO}/\text{NF}$ in 1.0 M KOH solution with or without KF (0.01 M).

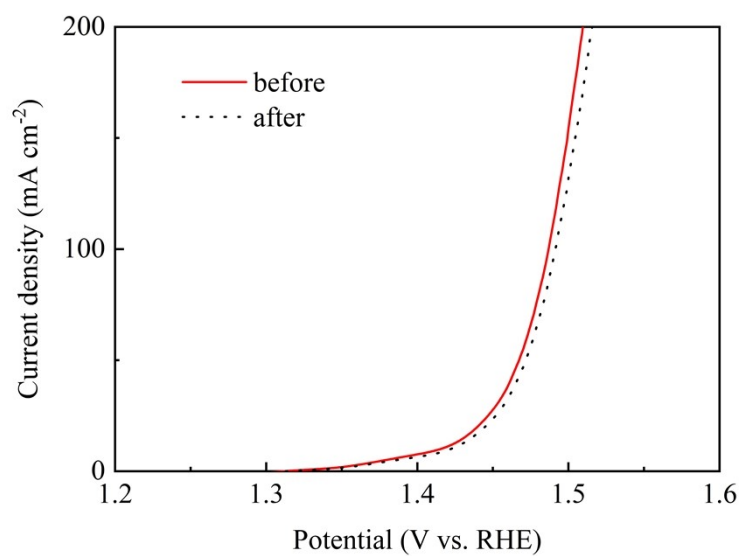


Fig. S6. The OER polarization curves of $\text{Ni}_{1-x}\text{Fe}_x\text{O}(\text{OH})_{1-y}\text{F}_y/\text{NiO}/\text{NF}$ before and after long-term operation at 500 mA cm^{-2} .

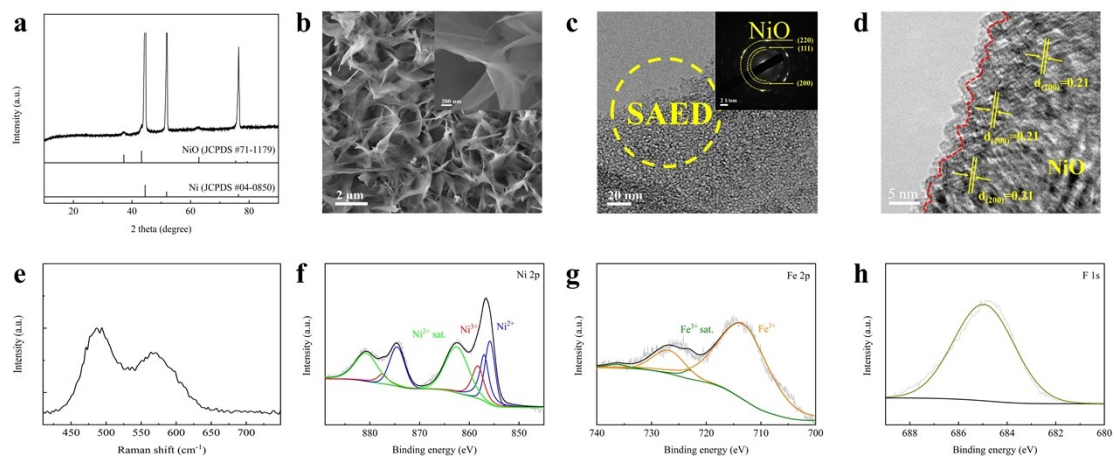


Fig. S7. (a) XRD pattern, (b) SEM images, (c) TEM image and the corresponding SAED pattern (inset), (d) HRTEM image, (e) Raman spectrum and (f-h) XPS spectra of the post-used $\text{Ni}_{1-x}\text{Fe}_x\text{O}(\text{OH})_{1-y}\text{F}_y/\text{NiO}/\text{NF}$ in a 1.0 M KOH+0.01 M KF electrolyte.

Table S1. EXAFS fitting parameters at the Ni K-edge for various samples ($S_0^2=0.77$)

Sample	Path	CN ^a	R(Å) ^b	$\sigma^2(\text{Å}^2)$ ^c
Ni _{1-x} Fe _x O(OH) _{1-y} F _y /NiO	Ni-O	6.1±0.1	2.01±0.01	0.0109
	Ni-Ni	6.4±0.2	2.94±0.01	0.0138
NiO(OH) _{1-y} F _y /NiO	Ni-O	6.3±0.2	2.00±0.01	0.0132
	Ni-Ni	6.7±0.3	2.92±0.01	0.0125
NiOOH/NiO	Ni-O	6.4±0.1	2.05±0.01	0.0079
	Ni-Ni	6.7±0.2	2.93±0.01	0.0118

^aCN: coordination number;

^bR: distance between absorber and backscatter atoms;

^c σ^2 : Debye-Waller factor to account for both thermal and structural disorders.

Table S2. EXAFS fitting parameters at the Fe K-edge for various samples ($S_0^2=0.79$)

Sample	Path	CN ^a	R(Å) ^b	$\sigma^2(\text{Å}^2)$ ^c
Ni _{1-x} Fe _x O(OH) _{1-y} F _y /NiO	Fe-O	4.4±0.1	1.93±0.01	0.0053
	Fe-Fe(Ni)	2.1±0.9	2.96±0.02	0.0129
FeOOH	Fe-O	5.1±0.4	1.97±0.02	0.0071
	Fe-Fe	6.1±0.7	3.04±0.01	0.0114

^aCN: coordination number;

^bR: distance between absorber and backscatter atoms;

^c σ^2 : Debye-Waller factor to account for both thermal and structural disorders.

Table S3. A comparison of the OER activities of various electrocatalysts.

Catalyst	η (mV) at 10 mA cm^{-2}	Electrolyte	Ref.
Fe-doped $\beta\text{-Ni(OH)}_2/\text{NF}$	219	1.0 M KOH	1
$\text{NiFe}_2\text{F}_{4.4}\text{O}_{1.8}$	270	1.0 M KOH	2
F-CoOOH/NF	270	1.0 M KOH	3
NiFe LDH NSA/IF	269	1.0 M KOH	4
$\text{Ni}_{1-x}\text{Fe}_x$ LDH/NF	217	1.0 M KOH	5
NiFe-LDH HMS/NF	239	1.0 M KOH	6
S-NiCoFe LDH/CC	206	1.0 M KOH	7
A-NiFe-OH/NiFeP/NF	199	1.0 M KOH	8
P- $\text{Ni}_{0.75}\text{Fe}_{0.25}\text{Se}_2/\text{CC}$	185	1.0 M KOH	9
D-NiFe/NF	172	1.0 M KOH	10
$\text{Ni}_{1-x}\text{Fe}_x\text{OOH}/\text{NiO}/\text{NF}$	225	1.0 M KOH	This work
$\text{Ni}_{1-x}\text{Fe}_x\text{O(OH)}_{1-y}\text{F}_y/\text{NiO}/\text{NF}$	186	1.0 M KOH	This work

References

- [1] T. Kou, S. Wang, J. L. Hauser, M. Chen, S. R. J. Oliver, Y. Ye, J. Guo, Y. Li, *ACS Energy. Lett.*, 2019, 4, 622-628.
- [2] K. Lemoine, J. Lhoste, A. Hemon-Ribaud, N. Heidary, V. Maisonneuve, A. Guiet, N. Kornienko, *Chem. Sci.*, 2019, 10, 9209-9218.
- [3] P. Chen, T. Zhou, S. Wang, N. Zhang, Y. Tong, H. Ju, W. Chu, C. Wu, Y. Xie, *Angew. Int. Ed. Chem.*, 2018, 57, 15471-15475.
- [4] Y. Liu, X. Liang, L. Gu, Y. Zhang, G. D. Li, X. Zou, J. Chen, *Nat. Commoun.*, 2018, 9, 2609.
- [5] G. Rajeshkhanna, T. I. Singh, N. H. Kim, J. H. Lee, *ACS Appl. Mater. Interfaces*, 2018, 10, 42453-42468.
- [6] C. Zhang, M. Shao, L. Zhou, Z. Li, K. Xiao, M. Wei, *ACS Appl. Mater. Interfaces*, 2016, 8, 33697-33703.
- [7] L. M. Cao, J. W. Wang, D. C. Zhong, T. B. Lu, *J. Mater. Chem. A* 2018, 6, 3224-3230.
- [8] H. Liang, A. N. Gandi, C. Xia, M. N. Hedhili, D. H. Anjum, U. Schwingenshlögl, H. N. Alshareef, *ACS Energy Lett.*, 2017, 2, 1035-1042.
- [9] Y. Huang, L. W. Jiang, B. Y. Shi, K. M. Ryan, J. J. Wang, *Adv. Sci.*, 2021, 8, 2101775.
- [10] C. Chen, P. Zhang, M. Wang, D. Zheng, J. Chen, F. Li, X. Wu, K. Fan, L. Sun, *ChemSusChem*, 2020, 13, 5067-5072.